Adam, B. and Smith, I.F.C. "Self-Diagnosis and Self-Repair of an Active Tensegrity Structure" Journal of Structural Engineering, Vol 133, 2007, pp 1752-1761. http://cedb.asce.org

Self Diagnosis and Self Repair of an Active Tensegrity Structure

Bernard Adam[1] and Ian F.C. Smith, F.ASCE[2]

Abstract

This paper addresses the study of tensegrity active control in case of unknown events, such as applied loading or damage. It describes methodologies for self diagnosis and self repair. Response due to unknown events is measured and analyzed in order to support self diagnosis. Since tensegrities are self-stressed and flexible structures, they exhibit geometrical non-linear behavior. Applied loading and damage thus induce changes in structural response to perturbations. This property is also used to support self diagnosis. Self-diagnosis solutions result in sets of good candidate description of the unknown event. Candidate descriptions exhibit responses to unknown events and perturbations that are close to the response measured on the real structure. These solutions are successfully employed within the framework of shape control and self repair. Self-repair abilities are demonstrated through increasing stiffness and decreasing stresses with respect to the damaged state by modifying the self-stress state of the structure. Validity of the results is demonstrated experimentally on a full-scale active tensegrity structure. The proposed methodologies are attractive for tensegrity active control in situations of unknown events.

CE Database subject headings: space structures, structural control, diagnosis, adaptive systems.

[1]PhD Student, Structural Engineering Institute, Ecole Polytechnique Fédérale de Lausanne (EPFL), Station 18, 1015 Lausanne, Switzerland. E-mail: bernard.adam@a3.epfl.ch

[2]Professor, Structural Engineering Institute, Ecole Polytechnique Fédérale de Lausanne (EPFL), Station 18, 1015 Lausanne, Switzerland. E-mail: ian.smith@epfl.ch

Introduction

Most civil structures are passive and static. They are designed according to serviceability criteria and to resist extreme situations. While they deflect in a passive manner, they do not adapt actively to external loading. A more challenging functionality of civil structures is that they react and adapt actively to changing requirements, such as new loading and eventual damage. Sobek and Teuffel (2002) performed numerical studies on the control of lightweight structures that react to external stimuli, such as varying loadings or noise. Pawlowski and Holnicki-Szulc (2004) introduced a structure that could adapt to extreme loads. It detected impacts through a set of sensors and optimally distributed forces in the structure using structural fuses. Anshuman and Kumar (2005) analyzed a set of intelligent building façades from a social-psychology perspective. However no experimental study has demonstrated self diagnosis and self repair in civil structures.

While structures that exhibit bionic behavior are an emerging research topic in civil engineering, bio-inspired systems have already been studied in domains such as electronics and informatics. The mathematician John Von Neumann (1966) is considered to be the pioneer of bionics. He proposed an automat that could self-repair and self-reproduce. Teuscher et al. (2003), Mange et al. (1999) and (1997), and Sipper et al. (1997) studied a fault-tolerant "Bio-Watch" that exhibited self-repairing characteristics and interacted with its environment. In computer science, Sterritt et al. (2005) postulated that autonomic computing systems are useful since they continue to be useful as conditions change. However, these examples come from virtual worlds of information science whereas civil structures exist in the physical environment.

Since tensegrities can be equipped with active control systems, they have the potential to exhibit bionic behavior. Tensegrities are lightweight and flexible structures. Stability is provided by the self-stress state between a tensioned cable net and compressed strut elements (Motro 1984). Shape control involves self-stress state modification in order to satisfy a serviceability objective (Shea et al, 2002, Fest et al, 2004; Domer and Smith, 2005). Few other studies have focused on tensegrity control. Kawaguchi et al. (1996) studied shape and stress control of prestressed truss structures. Difficulties were identified in validating numerical results through experimental testing. Averseng and Crosnier (2004) studied the control of a tensegrity grid in which the actuation system is connected to the supports. Other studies of tensegrity control involve only numerical simulation. Van de Wijdeven and de Jager (2005) proposed an example of 2D tensegrity vibration and shape control. Kanchanasaratool and Williamson (2002) proposed a dynamic model to study tensegrity feedback shape control. Skelton et al. (2000) concluded that since only small amounts of energy are needed to change the shape of tensegrity structures, they are advantageous for active control. Sultan (1999) proposed a formulation of tensegrity active control and illustrated it with the example of an aircraft motion simulator. Djouadi et al. (1998) described a theoretical scheme to control vibrations of tensegrity systems.

Damage tolerance of tensegrities is a new research area. It is often assumed that local damage would cause a catastrophic collapse. Appropriate topologies have recently been demonstrated to tolerate local damage. Fu (2005) studied the failure modes of tensegrity domes and proposed design methods. Lazopoulos (2005) analytically studied the buckling of a strut in an elastic 6-strut and 24-cable tensegrity module and described its post-critical behavior. While these structures are damage tolerant, they do not have capabilities for self repair.

Self diagnosis is supported by system identification through model-based diagnosis. System identification involves determining the state of a system as well as values of key parameters through comparisons between predicted and observed responses (Ljung 1999). Thus, system identification is an attempt to solve an inverse engineering task. Causes have to be inferred from measured effects (Raphael and Smith 2003a). In structural engineering, this research area can be divided into three sub-areas: damage identification (Park et al. 2005), load identification (Vanlanduit et al. 2005) and structural property identification (Haralampidis et al. 2005). However these three areas have been validated only on simple structures. Only Maeck and DeRoeck (2003) and Logamarsino and Calderini (2005) tested their methodologies on full-scale civil structures. Errors due to measurement precision and modeling assumptions influence results. Solutions are usually a set of good candidate models rather then one single solution (Robert-Nicoud et al. 2005). Most of these studies focus on health monitoring tasks that do not extend to control in case of unknown events.

This paper describes how self diagnosis, shape control and self repair can be integrated into tensegrity active control in cases of unknown events. Self diagnosis involves either loading identification or location of damage. Self-diagnosis solutions are used for control tasks such as shape control or self repair. Self repair involves stiffness increases and stress decreases with respect to damage state. Previous work at EPFL in the area of active tensegrity structures is reviewed in the following section. The following section on self diagnosis and self-repair describes new methodologies. Results and observations from experimental validation of these proposed methodologies are then discussed. The paper concludes with a discussion of the limitations of these methods, future work and conclusions.

Previous work at EPFL

Research into active structures has been carried out at EPFL since 1996. The structure is composed of 5 modules and rests on three supports (Figure 1). It covers a surface area of 15 m^2, has a static height of 1.20 m and withstands a distributed dead load of 300 N/m^2. It is composed of 30 struts and 120 tendons. Struts are fiber reinforced polymer tubes of 60mm diameter and 703 mm^2 cross section. Tendons are stainless steel cables of 6 mm in diameter. The central node and star topology is a particularity of each module. This topology was first proposed by Passera & Pedretti, Lugano (Switzerland) to limit buckling lengths, thereby allowing more slender compression elements than more traditional tensegrity. The structure is equipped with an active control system: ten actuators change length of compressed struts and three displacement sensors measure vertical displacements at three nodes of the top surface edge. Fest (2002) contains a description of the laboratory structure and the control system. Shape control involves satisfying a serviceability objective: maintaining the slope of the top surface of the structure when the structure is subjected to a load. Slope is determined through vertical displacement measurements at three nodes: 37, 43 and 48 (Figure 2). This objective is a control criterion that could be useful for structures such as antennas, pedestrian bridges and temporary roofs. The most challenging part of the study is the determination of control commands (sequence of contractions and elongations of active struts) that modify the self-stress state in order to satisfy this objective. Since behavior is geometrically non linear and highly coupled, there is no closed form solution for actuator movements given a required slope (Fest et al. 2003). A single objective stochastic search algorithm (Raphael and Smith, 2003b) was selected as the best method to accommodate the exponentially complex generate-test process that is needed to find control commands (Domer et al. 2003).

Domer and Smith (2005) studied the capacity of the structure and its control system to learn. Stochastic search is a generate-test strategy. Case-based reasoning was used to speed up the process. In order to take advantage of previous experience, previously successful control commands are stored in a case-base. When the structure is subjected to a load, a similar configuration is retrieved from the case base and its control command is adapted to the new task. As more cases are added to the case-base, the average time necessary to identify and adapt a control command decreases (Domer 2003). Since the structure is able to improve performance progressively using past experience, the structure learns.

Adam and Smith (2006) proposed a multi-objective approach to support tensegrity shape control. Since more robust control commands were identified using this approach than with single objective control, the structure was observed to accommodate multiple loading events over its service life.

In these previous studies, it was assumed that the load position and magnitude were known. However, these studies focused only on applied load cases and did not consider damage location and repair. Self diagnosis and self-repairing aspects are reviewed in the following section. Experimental results provide validation of the methodologies.

Self diagnosis

For the purpose of this paper, self diagnosis involves identifying load positions and magnitudes in cases of unknown applied loads, and damage location in cases of unknown damage. The methodology involves measuring and analyzing response of the structure to unknown events. Since tensegrities are self-stressed and flexible structures, they exhibit non-linear behavior. Perturbations are applied through small actuator elongations. Damages and

applied loads induce changes in response to perturbations. Such changes are measured to support self diagnosis. Self diagnosis solutions are used to identify control commands in order to either control shape or self repair. In cases of applied loading, the control objective, is to satisfy the serviceability criterion of maintaining the value for top surface slope of the structure (Figure 3). In cases of structural damage, safety objectives become more relevant than serviceability. Self-repairing abilities are demonstrated as follows. To improve the safety of the damaged structure, the safety objective involves stiffness increases and stress decreases.

System identification supports self diagnosis. This technique requires neither intensive measurements nor the use of force sensors. The methodology is based on comparing measured and numerical responses with respect to three indicators that reflect changes in structure response: top surface slope deviation, transversal rotation and influence vector. These three indicators are presented below:

- Top surface slope deviation *S*: Since maintaining the top surface slope is the main shape control objective, it is also used as the main indicator (Figure 2):

$$S = \frac{\left(z'_{43} - \frac{z'_{37} + z'_{48}}{2}\right) - \left(z_{43} - \frac{z_{37} + z_{48}}{2}\right)}{L}$$

  where z'_i is the vertical coordinate of node *i* event, z_i the vertical coordinate of node *i* before event and *L* the horizontal distance between node 43 and the middle of segment 37 – 48 (Figure 2). The slope units used throughout this paper are mm/100m. Zero slope deviation means that top surface slope is equal to initial top surface slope.

- Transversal rotation, *R*: This second indicator is expressed as the rotation of segment 37 – 43 (Figure 2):

$$R = \left(z'_{48} - z'_{37}\right) - \left(z_{48} - z_{37}\right)$$

According to this definition, clockwise rotations are positive.

- Top surface slope variations are induced by perturbations. They are formally expressed as follows:

$$\Delta S = S'' - S'$$

where S'' is the slope after perturbation and S' is the slope before perturbation. In the present study, perturbations are defined as a 1 mm elongation of actuators (Figure 2). Slope variations induced by each of the 10 actuators are put together in order to create influence vectors $\boldsymbol{v}$. The influence vector is the third indicator. These vectors express the slope variation per mm of actuator elongation:

$$\boldsymbol{v} = \left[\Delta S(1) \quad \cdots \quad \Delta S(10)\right]^T$$

where $\Delta S(i)$ is the slope variation per mm of elongation of actuator i. Since tensegrities are self-stressed and flexible structures, applied loads and damages cause non-linear behavior. Effects are observed through modifications of influence vector.

Load identification

The load identification involves magnitude evaluation and load location. The methodology uses the three aforementioned indicators (Figure 4). In this study, loading is assumed to be single static vertical point loads. They are applied one at a time on one of the 15 top surface nodes (Figure 2). While the algorithm in this section is able to identify only single loads, a generalization of this algorithm to more complex loading is future work.

The following steps lead to load identification:

Step 1: Top surface slope deviation is the first indicator. Once loaded magnitude evaluation involves numerically determining, for each of the 15 nodes, which load magnitude can induce the same slope deviation as that measured on the laboratory structure. Dynamic relaxation

(Barnes 1977) is used for numerical simulation. This evaluation is performed iteratively for each node (Figure 2). Load magnitude is gradually increased until the numerically calculated slope deviation is equal to the measurement. The load is incremented in steps of 50N. Loaded nodes inducing a slope deviation in the inverse direction than the one measured are not considered. Load magnitudes and locations create a set of candidate solutions.

Step 2: Transversal rotation is the second indicator. The candidate solutions that exhibit inverse transversal rotation with respect to laboratory structure measurements are rejected. Experimental measurements show that 0.1mm is an upper bound for precision error for transversal rotation. In cases where transversal rotation is less than 0.1mm, no candidate solutions are rejected.

Step 3: The influence vector is the third indicator. It includes slope variations per mm of actuator elongations. The influence vector is evaluated for the laboratory structure through perturbations and slope variation measurements. For remaining candidate solutions, the influence vector is evaluated through numerical simulation of perturbations. The candidate influence vector that exhibits the minimum Euclidian distance with the influence vector of the laboratory structure subjected to the load indicates the candidate that is the closest to the laboratory structure. It is taken to be the reference candidate.

$$\min\left|\boldsymbol{v}_{can} - \boldsymbol{v}\right| = \min\left(\sqrt{\sum_{j=1}^{10}\left(\Delta S_{can}(j) - \Delta S(j)\right)^2}\right)$$

where $\Delta S_{can}(j)$ is the numerically calculated slope variation of a candidate for perturbation applied through actuator j, $\Delta S(j)$ the measured slope variation for the perturbation applied through actuator j on the laboratory structure. Practical applications of system identification include consideration of errors. An upper bound for the error on slope variations for one single perturbation, e_p, has been observed to be e_p = 0.11 mm/100m. This error is related to variations in the actuation system and sensor system accuracy. Candidate solutions for which

the Euclidian distance with the reference candidate is less the 10 times e_p are also considered load identification candidate solutions.

$$\left| \boldsymbol{v}_{ref} - \boldsymbol{v}_{can} \right| \leq 10 \cdot e_p$$

This process results in a set of "good" candidate solutions. For each of these solutions, load magnitudes are modified to approach more closely measured top surface slope deviation with 10 N increments. Improved candidates create the load identification solution set. In this set, candidate solution responses are close to the measured response of the laboratory structure. These solutions are used as input to identify a control command for the shape control task (Adam and Smith 2006).

Damage location

Traditional tensegrities do not exhibit redundant load path behavior. Rupture of one single element usually leads to catastrophic collapse. In this structure, module topology and module connections provide redundancy. The basic module contains more cables than the number required to provide stability. Moreover, module connection is provided by multiple cables and nodes. Since loads can follow multiple paths, the structure is redundant and consequently there is potential for tolerating and locating damage.

Redundancy is quantified numerically. Cases of damage are simulated using dynamic relaxation. Damaged elements leading to structural collapse or progressive collapse through either strut buckling, loss of compression in a strut or cable rupture are called critical elements. Only one tenth of cables and the struts are critical elements (Figure 5). Critical cables are mostly located at the edge of the structure where loads can not pass through other elements without causing a failure. In cases of non critical element failure, the position of the broken element is identified through the damage location methodology described next.

In a similar way to the task of load identification, top surface slopes and influence vectors are used as indicators (Figure 6). Local damage induces top surface slope deviation. Slope deviation is measured on the damaged laboratory structure. Within the framework of damage location, a candidate is defined as the structure with one cable broken. A generalization of the proposed algorithm for more complex structures and damage is presented in the future work section. The following steps are carried out:

Step 1: There are 91 non-critical elements in the structure. 91 candidates that correspond to the 91 non-critical elements in the structure are considered. A maximal error of e_s = 96 mm/100m has been observed for slope deviation between the laboratory structure and numerical models in cases of damage. Candidate solutions that show an absolute value of the difference between measured slope deviation and candidate slope deviation that is less than this error, are retained.

$$\left|S'_m - S'_c\right| \leq e_s$$

where S'_m indicates the measured slope deviation and S'_c the calculated slope deviation of the candidate.

Step 2: The influence vector is used as the second indicator. Perturbations are applied to the damaged structure and to numerical models of candidate solutions. Candidates for which perturbations induce instability are not considered. The candidate with the minimum Euclidian distance between its influence vector and the influence vector of the damaged structure is taken to be the reference candidate. Its response to perturbations is the closest to the response of the laboratory structure. Since precision errors are considered, other candidate solutions for which the Euclidian distance between their influence vector and the influence vector of the reference candidate is less than the upper bound of slope variation error for 10 perturbations are also taken to be good candidate solutions. These solutions are a set of

solutions whose response is close to the response of the damaged laboratory structure. These good candidate solutions are used as input to identify a control command for self-repair task.

Self Repair

In case of damage, safety becomes more important than serviceability. Self-repair measures have priority. The control objective is thus modified. The safety objective involves stiffness increases and stress decreases with respect to damage state. Since stiffness increase and stress decrease are conflicting objectives, a multi-objective search method is attractive to identify control commands that maximizes safety. For the purposes of this study, the structure approximate global stiffness indicator is expressed as follows:

$$K = \frac{Q_{37} + Q_{43} + Q_{48}}{\left|\Delta S(Q_{37})\right| + \left|\Delta S(Q_{43})\right| + \left|\Delta S(Q_{48})\right|}$$

where $\Delta S(Q_i)$ is the slope variation induced by the vertical point load Q_i = 1000 N, at node i. Since Q_i is expressed in N and $\Delta S(Q_i)$ in mm/100m, approximate global stiffness indicator unit is $N/(mm/100m)$.

Minimizing stress involves minimizing the stress in the element of the structure that is the closest to its capacity:

$$T = \max\left(\frac{N}{N_{\lim}}\right)$$

where N is the stress in cable and $N_{\lim}$ the cable capacity. Previous studies showed that cables are always closer to their capacity than struts.

To avoid subjectivity related to weight coefficients, a Pareto approach (Pareto 1896) is proposed to support multi-objective search for a self-repairing control command. Sets of Pareto optimal solutions are built according to stiffness and stress objectives. The

serviceability objective is of tertiary importance. Among the set of Pareto optimal solutions, the solution that exhibits the greatest slope compensation is selected to be the self repairing control command.

Experimental testing, results and observations

The proposed methodologies are validated through experimental testing on a full-scale active tensegrity structure (Figure 1).

Load identification and shape control

The load identification methodology is tested experimentally for 11 load cases (Table 1). These load cases are arbitrary applied to the top surface nodes (Figure 2). Their magnitudes range from 391 N to 1209 N. These loads represent a wide spectrum of possibilities.

For example, examine load case 5. The laboratory structure is loaded with 859 N at node 32. Top surface slope deviation is the first indicator. The measured slope deviation is equal to 133.6 mm/100m. In 7 top surface nodes out of 15, downward point loads can induce a slope deviation that is close to the one measured. This creates 7 candidate solutions which are listed in Table 2.

Transversal rotation is the second indicator. The load on the laboratory structure induces a counterclockwise transversal rotation. Since candidates 1 and 2 exhibit clockwise transversal rotation, they cannot be solutions and are rejected.

The influence vector is used as the third indicator. It contains top surface slope variation per mm of actuator elongations. Slope variations result from perturbations. The 10 actuators used for perturbations are indicated in Figure 2. Slope variations are presented in Table 3. Perturbations are numerically simulated on remaining candidate solutions of Table 2. Slope

variations and Euclidian distance between laboratory structure influence vector and candidate solution influence vectors are presented in Table 4.

Euclidian distance between influence vectors indicates the similarity between laboratory structure and candidate solutions. Similarity is maximal when this Euclidian distance is minimal. It is minimal for candidate 4, 800 N at node 32. In other words, candidate 4 exhibits the closest response to the response measured on the laboratory structure subjected to perturbations. This is the reference candidate. The reference candidate Euclidian distance is equal to 6.7 mm/100m. Considering precision errors of the active control system, candidate solutions 5 and 6, 1050 N at node 51 and 500 N at node 48, both with Euclidian distances equal to 7.1 mm/100m are also accepted as solutions.

Finally these three candidate solutions are improved by approaching the measured slope deviation with load magnitude increments of 10 N. The three solutions of load case identification are presented in Table 5.

For these three solutions, control commands for slope compensation are identified using a multi-objective search algorithm (Adam and Smith 2006). The three control commands are applied to the laboratory structure. Slope compensation is defined to be the ratio between measured correction induced by the control command application and the initial slope deviation. It ranges between 91 % and 95 %, even if the control command is identified with a load identification solution that is not exactly the real applied load. These three solutions are considered equivalent (Figure 7). Slope deviation evolution is plotted against steps of 1mm of actuator travel. In this case, the best slope compensation of 95 % corresponds to the closest candidate: 770 N at node 32.

In order to generalize the results presented above, load case identification and slope compensation are performed on the 11 load cases listed in Table 1. Results are summarized in Table 6. The following observations can be made on the basis of these results:

- In each of these sets, dispersion in top surface slope compensation is less than 15 %. Since this value is close to the slope deviation precision error, load identification solutions are considered to be equivalent.
- The closest candidate is not always the one that is located at the same node as the applied load case.
- The exact load location does not always lead to the best top surface slope compensation.

These observations demonstrate the validity of examining a set of good solutions instead of the best solution with respect to a particular indicator. It also reveals the robustness of the methodology. In case of structural changes such as cable relaxation or support movements, a set of solutions that are the closest to the real structure configuration are identified.

For maintaining robustness of the control system (Adam and Smith 2006), in each of these sets, the shortest control command is used for slope compensation. In other words, the control command for which the sum of the actuator strokes is minimal is applied to the laboratory structure. The corresponding slope compensation for each load case is presented in Figure 8. Slope compensation is better than 84 % for all load cases except for load case 7. Since slope compensation quality is evaluated at final state without taking into account the control command sequence application, load case 7, which exhibits high value of initial slope deviation, is an exception. Non-linear effects observed during control command applications become more significant when control commands are long.

Damage location

The effectiveness of the damage location is reviewed in this section. Consider that cable 7 is broken. Top surface slope deviation is the first indicator. The slope deviation is measured on the laboratory structure. It is equal to 256 mm/100m. Among all possibilities, two candidate solutions induce a slope deviation that is close to the one measured on the laboratory structure (Table 7).

Influence vector is the second indicator. It contains slope variations induced by perturbations on the laboratory structure. Slope variation values are measured and listed in Table 8. Slope variations due to perturbations are numerically simulated on the two remaining candidate solutions. Slope variation values and Euclidian distances are presented in Table 9.

Euclidian distance is minimal for candidate 2: cable 43 broken. This candidate exhibits the closest response to the laboratory structure due to perturbations. It is considered to be the reference candidate. Reference candidate Euclidian distance is equal to 6.9 mm/100m. Considering errors, candidate 1, cable 7 broken, is also considered to be a good candidate solution for damage location with a Euclidian distance of 7.1 mm/100m. Candidates 1 and 2 are the set of damage location solutions. These two solutions are used to identify a self-repairing control command.

Self Repair

As described earlier, the objectives of self-repair are to increase the stiffness and lower the stresses with respect to the damage state. Experimental validation is demonstrated by not having the cable 7 on the structure (Figure 5). Cable 7 is one of the most tensioned non critical cables. Damage location solutions are used to identify the self-repairing control command using the presented multi-objective search method. At initial state, stiffness indicator is equal to 3.92 N/mm/100m and maximal tension in cable elements is equal to 7.8

kN. When cable 7 breaks, stiffness indicator falls to 3.56 N/mm/100m and highest tension increases up to 9.0 kN. Self repair increases stiffness indicator up to 3.78 N/mm/100m with the control command identified for cable 7 broken, 3.70 N/mm/100mm with the control command identified for cable 43 broken, respectively. The highest tension decreases to 8.8 kN with the control command identified for cable 7 broken, 7.9 kN with the control command identified for cable 43 broken, respectively. The effects of damage and self repair are summarized in Figure 9 for the case when cable 7 is broken. Stiffness indicator values are experimental values, whereas stress values are numerical values only because the laboratory structure was not equipped with strain sensors. As the maximum value of the tension in the cables decreases during self-repair, the maximum value of compression in the struts increases. This is permitted since reserve capacity is higher in struts than in cables.

Limitations and Future Work

A more general implementation of the self diagnosis algorithm, with variable parameters for elements stiffness, support conditions, node friction and the use of stochastic search may lead to better solutions for more complex structures. A general representation of load case types, such as two or more point loads, continuous loads and lateral loads would also be attractive for the self-diagnosis algorithm. Self-diagnosis results revealed opportunities for control command learning that lead to two types of learning: reduction of control command identification time and increase of control command quality over time.

Conclusions

Self diagnosis, including load identification and damage location, provides solutions that are used efficiently for shape control and self-repair. More specifically, the following conclusions come out of the study on self diagnosis:

- System identification algorithms contribute to self-awareness in active structures and leads to successful self diagnoses.
- Non linear response to applied loads and damage is successfully evaluated to support self diagnosis.
- Experimental testing justifies the strategy of initial generation of a set of good solutions rather than direct (and often erroneous) assignment of one single solution.

In cases of damage, safety becomes more important than serviceability. The following conclusions come out of the study on self repair:

- Self-repairing abilities are successfully demonstrated through increasing stiffness and decreasing stresses with respect to the damaged state.
- The possibility of controlling other objectives such as stiffness and stress by modifying the self-stress state of an active tensegrity structure is demonstrated.
- The topology of the tensegrity structure in this study allows for redundant load-path behavior for some types of damage.

The methodologies described in this paper are particularly attractive for active control in situations where there may be unanticipated applied loading and damage.

Acknowledgments

The authors would like to thank the Swiss National Foundation for supporting this work. They also thank B. Domer, P. Kripakaran and B. Rebora for discussions and advice. B. Domer also improved control and implemented the case-based reasoning study. E. Fest built the structure and the control system. B. Raphael provided support during programming of the control system. We are also grateful to Y. Robert-Nicoud for his advice, Passera & Pedretti SA (Lugano, Switzerland), Lust-Tec GmbH (Zürich, Switzerland) and P. Gallay for their contributions.

Notation

The following symbols are used in this paper:

S = Top surface slope deviation

z_i = Vertical coordinate of node i, at initial state

z'_i = Vertical coordinate of node i, after unknown event occurrence

L = Horizontal distance between node 43 and the middle of segment 37 - 48

R = Transversal rotation

ΔS = Top surface slope variation

S'' = Slope deviation after perturbation

S' = Slope deviation before perturbation

$\boldsymbol{v}$ = Influence vector

$\boldsymbol{v}_{can}$ = Influence vector of a candidate

ΔS_{can} = Numerically calculated top surface slope variation of a candidate for a perturbation

e_p = Upper bound error on top surface slope variation for one single perturbation, between the laboratory structure and numerical models

$\boldsymbol{v}_{ref}$ = Influence vector of reference candidate

e_s = Upper bound error on top surface slope deviation between the laboratory structure and numerical models due to damage

K = Global stiffness indicator

T = Ratio between stress and capacity of the element that is the closest to its capacity

N = Normal force

N_{lim} = Normal force capacity

References

Adam, B. and Smith, I.F.C., (2006), "Tensegrity Active Control: a Multi-Objective Approach", Journal of Computing in Civil Engineering, accepted.

Anshuman, S. and Kumar, B., (2005), "Intelligent Building Façades; Beyond Climatic Adaptivity", Computing in Civil Engineering, Proceedings of the 2005 ASCE Computing Conference, American Society of Civil Engineers, Reston VA, USA, 2005, CDROM.

Averseng, J., and Crosnier, B., (2004), "Static and Dynamic Robust Control of Tensegrity Systems", Journal of The International Association for Shell and Spatial Structures, 45, 169-174.

Barnes, M.R., (1977), "Form Finding and Analysis of Tensioned Space Structures by Dynamic Relaxation", PhD Thesis, The City University of London, London.

Djouadi, S., Motro, R., Pons, J.C., and Crosnier, B., (1998), "Active Control of Tensegrity Systems", Journal of Aerospace Engineering, 11, 37-44.

Domer, B., and Smith, I.F.C., (2005) "An Active Structure that learns", Journal of Computing in Civil Engineering, 19(1), 16-24.

Domer, B., Raphael, B., Shea, K. and Smith, I.F.C. (2003), "A study of two stochastic search methods for structural control", Journal of Computing in Civil Engineering, 17(3), 132-141.

Domer, B., (2003). "Performance enhancement of active structures during service lives", Thèse no 2750, Ecole Polytechnique Fédérale de Lausanne.

Fest, E., Shea, K., and Smith, I.F.C., (2004), "Active Tensegrity Structure", Journal of Structural Engineering, 130(10), 1454-1465.

Fest, E., Shea, K., Domer, B, and Smith, I.F.C., (2003), "Adjustable Tensegrity Structure", Journal of Structural Engineering, 129(4), 515-526.

Fest, E., (2002). “Une structure active de type tenségrité”, Thèse no 2701, Ecole Polytechnique Fédérale de Lausanne.

Fu, F., (2005), “Structural behavior and design methods of Tensegrity domes”, Journal of Constructional Steel Research, 61, 23-35.

Haralampidis, Y., Papadimitriou, C. and Pavlidou, M., (2005), “Multi-objective framework for structural model identification”, Earthquake Engineering and Structural Dynamics, 34, 665-685.

Kanchanasaratool, N., and Williamson, D., (2002), “Modelling and control of class NSP tensegrity structures”, International Journal of Control, 75(2), 123-139.

Kawaguchi, K., Pellegrino, S. and Furuya, H., (1996), “Shape and Stress Control Analysis of Prestressed Truss Structures”, Journal of Reinforced Plastics and Composites, 15, 1226-1236.

Lagomarsino, S. and Calderini, C., (2005), “The dynamical identification of the tensile force in ancient tie-rods”, Engineering Structures, 27, 846-856.

Lazopoulos, K.A., (2005), “Stability of an elastic cytoskeletal tensegrity model”, International Journal of Solids and Structures, 42, 3459-3459.

Ljung, L., (1999), System identification-theory for the users, Prentice-Hall, Englewood Cliff, N.J.

Maeck. J. and De Roeck, G., (2003), “Damage assessment using vibration analysis on the z24-bridge”, Mechanical Systems and Signal Processing, 17, 133-142.

Mange, D., Sipper, M. and Marchal, P., (1999), “Embryonic electronics”, BioSystems, 51, 145-152.

Mange, D., Madon, D., Stauffer, A. and Tempesti, G., (1997). “Von Neumann revisited: A Turing machine with self-repair and self-reproduction properties”, Robotics and Autonomous Systems, 22, 35-58.

Motro, R., (1984), “Forms and forces in tensegrity systems”, In:Nooshil, H. (Ed.), Proceedings of Third International Conference on Space Structures. Elsevier, Amsterdam, 180-185.

von Neumann, J. (1966), “The theory of Self-Reproducing Automata” University of Illinois Press, Urbana.

Pareto, V., (1896), “Cours d’Economie Politique”, vols I and II, Rouge: Lausanne, Switzerland.

Park, G., Rutherford, A.C., Sohn, H. and Farrar, C.R., (2005), “An outlier analysis framework impedance-based structural health monitoring”, Journal of Sound and Vibration, 286, 229-250.

Pawlowski, P. and Holnicki-Szulc, J., (2004), “Adaptive Structures under Extreme Loads – Impact detection, Self-adaptation, Self-repairing”, Proceedings of the Third European Conference on Structural Control, Vienna, Austria.

Raphael, B. and Smith, I.F.C., (2003a), Fundamentals of Computer-Aided Engineering, John Wiley & Sons Ltd, England.

Raphael, B. and Smith, I.F.C., (2003b) “A direct stochastic algorithm for global search”, J of Applied Mathematics and Computation, 146(2-3), 729-758.

Robert-Nicoud, Y., Raphael, B. and Smith, I.F.C., (2005), “System Identification through Model Composition and Stochastic Search”, Journal of Computing in Civil Engineering, 19(3), 239-247.

Sipper, M., Mange, D. and Stauffer, A., (1997), “Ontogenetic hardware”, BioSystems, 44, 193-207.

Shea, K., Fest, E. and Smith, I.F.C. (2002) "Developing intelligent tensegrity structures with stochastic search" Advanced Engineering Informatics, Vol 16, No 1, pp 21-40.

Skelton, R.E., Helton, J.W., Adhikari, R., Pinaud, J.P. and Chan, W., (2000), "An introduction to the mechanics of tensegrity structures", Handbook on mechanical systems design, CRC, Boca Raton, Fla.

Sobek, W. and Teuffel, P., (2002), "Adaptive Lightweight Structures", Proceedings of the International IASS Symposium, 24-28 June 2002, Warsaw, Poland. Ed. Obrebski, J. B., Wydawnicto Naukowe: Micro Publisher, 203-210.

Sterritt, R., Parashar, M., Tianfield, H. and Unland. R., (2005), "A concise introduction to autonomic computing", Advanced Engineering Informatics, 19, 181-187.

Sultan, C., (1999) "Modeling, design and control of tensegrity structures with applications", PhD thesis, Purdue Univ., West Lafayette, Ind.

Teuscher, C., Mange, D., Stauffer, A. And Tempesti, G. (2003). "Bio-inspired computing tissues: towards machine that evolve, grow, and learn", BioSystems, 68, 235-244.

Van de Wijdeven, J. and de Jager, B., (2005), "Shape Change of Tensegrity Structures: Design and Control", Proceedings of the American Control Conference, Protland, OR, USA, 2522-2527.

Vanlanduit, S., Guillaume, P., Cauberghe, B., Parloo, E., De Sitter, G. and Verboven, P., (2005), "On-line identification of operational loads using exogenous inputs", Journal of Sound and Vibration, 285, 267-279.

Figures

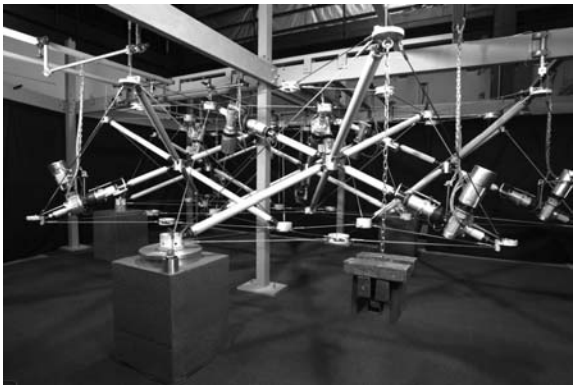

Fig. 1. 5 module, 15 m^2 active tensegrity structure used for tests

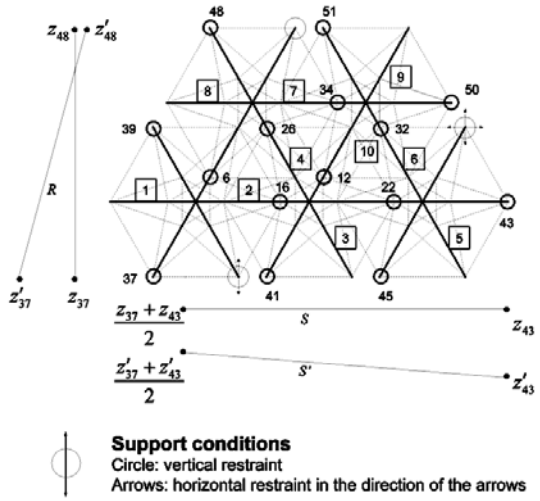

Fig. 2. View of the structure from the top with the 10 actuators numbered in squares and upper nodes indicated by a circle. Slope *S* and transversal rotation *R* are indicated. Lines represent the top surface from both sides.

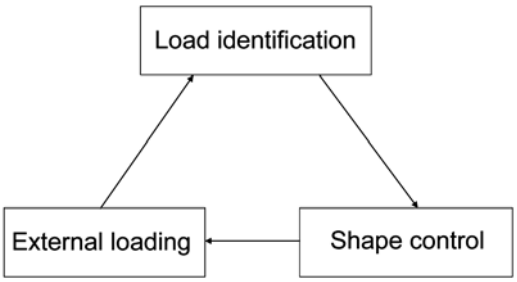

Fig. 3. Load identification and shape control in cases of applied loading

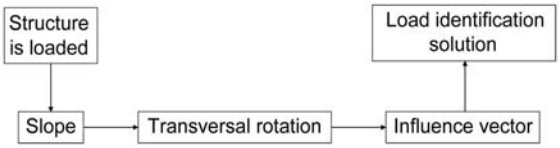

Fig. 4. Indicators involved in load identification process

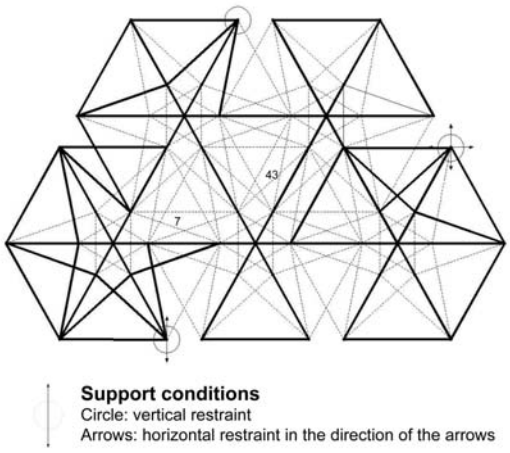

Fig. 5. Critical elements are indicated in bold

Fig. 6. Indicators involved in damage location process

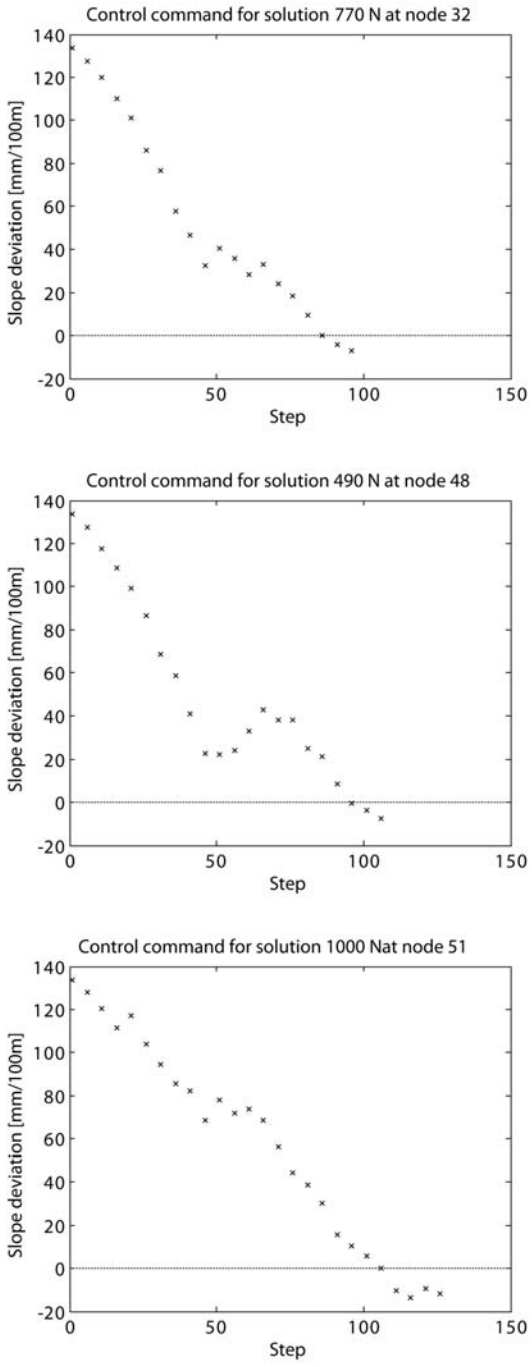

Fig. 7. Shape control for load case 5: 859 N at node 32, for the three load identification solutions: 770 N at node 32, 1000 N at node 51 and 490 N at node 48

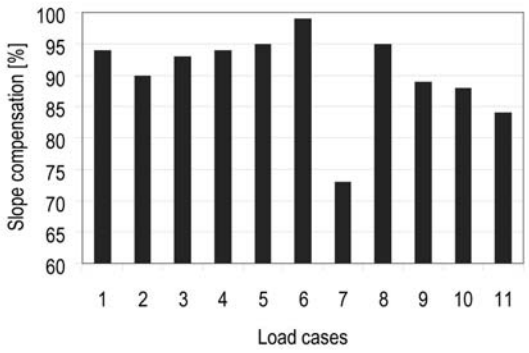

Fig. 8. Slope compensation for the 13 tested load cases

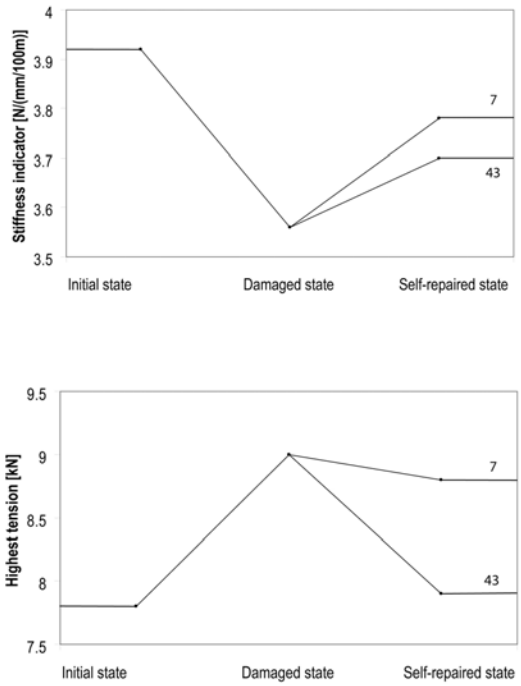

Fig.9. Damage effects and self-repair for broken cable 7 according to damage location solutions: cable 7 and cable 43

Tables

Table 1. Load Cases applied to the structure

Load Case	Loaded node	Load magnitude [N]
1	26	-625
2	26	-900
3	26	-1209
4	32	-625
5	32	-859
6	32	-1092
7	37	-550
8	48	-391
9	48	-550
10	48	-700
11	6	-1092

Table 2. Candidates with their numerically calculated slope deviation

Candidate	Node	Magnitude [N]	Slope deviation [mm/100m]	Trans. rotation
1	37	-550	144.1	1.3
2	39	-350	138.6	0.28
3	26	-850	134.6	-0.10
4	32	-800	137.4	-0.18
5	51	-1050	138.5	-0.81
6	48	-500	134.3	-1.18
7	6	-1450	135.3	-0.90

Table 3. Influence vector for load case 5 on the laboratory structure

Perturbation	Influence vector v [mm/100m]/mm
1	6.0
2	7.2
3	-9.4
4	-7.4
5	-12.6
6	-12.2
7	9.4
8	9.8
9	-4.3
10	-4.2

Table 4. Influence vector values and Euclidian distance for remaining candidates

	Influence vector v_{can} [mm/100m]/mm				
Perturbations	**Candidate 3**	**Candidate 4**	**Candidate 5**	**Candidate 6**	**Candidate 7**
1	9.7	9.9	9.2	10.0	12.0
2	9.7	9.9	9.2	10.0	12.1
3	-4.3	-6.3	-4.5	-5.4	-6.6
4	-4.3	-6.4	-4.5	-5.4	-6.6
5	-11.2	-14.2	-11.6	-13.5	-15.4
6	-11.0	-13.9	-11.3	-13.2	-15.1
7	10.6	11.2	10.2	11.2	13.3
8	10.5	11.2	10.1	11.1	13.2
9	-4.3	-5.4	-3.6	-4.4	-3.9
10	-4.2	-5.2	-3.5	-4.2	-3.7
$\lvert \boldsymbol{v}_{can} - \boldsymbol{v} \rvert$	7.9	6.7	7.1	7.1	10.6

Table 5. Self-diagnosis solutions for load case 5: 859 N at node 32

Candidate	**Node**	**Magnitude [N]**	**Slope deviation [mm/100m]**
4	32	-770	132.4
5	51	-1000	132.9
6	48	-490	131.6

Table 6. Summary of load identification solutions and shape control results

Applied load case		Self-diagnosis solution		Shape control result		
Loaded node	**Load magnitude [N]**	**Loaded node**	**Load magnitude [N]**	**Euclidian distance [mm/100m]**	**Slope compensation [%]**	**Sequence length [mm]**
26	-625	51	-540	5.6	83	17.1
		26	-470	6.1	89	18.1
		39	-190	6.1	98	18.1
		37	-290	6.5	95	20.3
		48	-280	6.5	94	13.2
26	-900	51	-730	5.6	90	14.7
		26	-620	6.1	100	19.8
26	-1209	51	-1010	1.8	93	18.7
		26	-850	2.0	94	19.9
32	-625	39	-270	5.5	88	21.0
		51	-780	5.6	82	15.9
		32	-620	6.0	92	16.6
		37	-410	6.0	91	18.6
		48	-400	6.0	96	16.3
		26	-660	6.2	94	15.5
32	-859	32	-770	6.8	95	15.5
		51	-1000	7.1	91	20.5
		48	-490	7.2	94	16.8
32	-1092	32	-980	6.3	97	18.6
		48	-620	7.0	99	18.4
37	-550	39	-350	5.9	74	17.7
		37	-530	6.0	73	16.3
48	-391	51	-700	5.2	95	13.0
		48	-360	6.0	88	15.4
		26	-600	6.1	94	17.0
		32	-560	6.2	80	17.9
48	-550	48	-510	5.5	94	16.9
		32	-810	6.0	89	13.1
48	-700	48	-660	6.6	88	20.0
		32	-1050	7.2	85	21.2
6	-1092	32	-610	4.3	84	13.9
		48	-390	5.4	89	16.1

Table 7. Candidate with slope deviation close to the measured one

Candidate	**Broken cable**	**Slope deviation [mm/100m]**
1	43	194
2	7	340

Table 8. Influence vector values for the laboratory structure damaged: cable 7 broken

Perturbation	Influence vector v [mm/100m]/mm
1	1.4
2	0.8
3	-1.7
4	-2.1
5	-3.7
6	-3.4
7	3.2
8	2.3
9	-1.0
10	-0.6

Table 9. Influence vector and Euclidian distance for remaining candidates

Perturbations	Influence vector v_{can} [mm/100m]/mm	
	Candidate 1	Candidate 2
1	6.3	3.4
2	5.6	3.4
3	-1.2	1.6
4	-1.2	1.6
5	-4.0	-2.8
6	-4.0	-2.8
7	3.6	1.1
8	3.6	1.0
9	-1.0	-2.3
10	-1.0	-2.3
$\lvert \boldsymbol{v}_{can} - \boldsymbol{v} \rvert$	7.1	6.9

Figure captions

Fig. 1. 5 module, 15 m^2 active tensegrity structure used for tests

Fig. 2. View of the structure from the top with the 10 actuators numbered in squares and upper nodes indicated by a circle. Slope *S* and transversal rotation *R* are indicated. Lines represent the top surface from both sides.

Fig. 3. Load identification and shape control in cases of applied loading

Fig. 4. Indicators involved in load identification process

Fig. 5. Critical elements are indicated in bold

Fig. 6. Indicators involved in damage location process

Fig. 7. Shape control for load case 5: 859 N at node 32, for the three load identification solutions: 770 N at node 32, 1000 N at node 51 and 490 N at node 48

Fig. 8. Slope compensation for the 13 tested load cases

Fig.9. Damage effects and self-repair for broken cable 7 according to damage location solutions: cable 7 and cable 43

Table captions

Table 1. Load Cases applied to the structure

Table 2. Candidates with their numerically calculated slope deviation

Table 3. Influence vector for load case 5 on the laboratory structure

Table 4. Influence vector values and Euclidian distance for remaining candidates

Table 5. Self-diagnosis solutions for load case 5: 859 N at node 32

Table 6. Summary of load identification solutions and shape control results

Table 7. Candidate with slope deviation close to the measured one

Table 8. Influence vector values for the laboratory structure damaged: cable 7 broken

Table 9. Influence vector and Euclidian distance for remaining candidates